RSC Advances

PAPER

View Article Online
View Journal | View Issue



Cite this: *RSC Adv.*, 2025, **15**, 42761

# Investigation of electrical transport mechanisms in an n-$CdIn_2Se_4$/Pt thin film Schottky diode fabricated by pulsed laser deposition

S. D. Dhruv, [a] Tanvi Dudharejiya,[b] Sergei A. Sharko,[c] Aleksandra I. Serokurova,[c] Nikolai N. Novitskii,[c] D. L. Goroshko,[d] Parth Rayani,[ae] Jagruti Jangale,[a] J. H. Markna, [b] Bharat Kataria[b] and D. K. Dhruv *[a]

This investigation focuses on the fabrication of an n-$CdIn_2Se_4$/Pt thin film Schottky diode using the pulsed laser deposition technique. The typical grazing incidence X-ray diffractogram displays a sharp and bright ⟨1 1 1⟩ characteristic reflection, confirming the formation of polycrystalline $CdIn_2Se_4$ thin films. Various microstructural parameters have been calculated for the $CdIn_2Se_4$ thin films using the most prominent ⟨1 1 1⟩ reflection. Hall measurement examination confirmed the n-type conductivity of the $CdIn_2Se_4$ thin films. Characterization of the voltage–current curve of the vacuum-fabricated n-$CdIn_2Se_4$/Pt thin film Schottky diode confirms the presence of a typical Schottky diode-type junction between $CdIn_2Se_4$ and platinum with a good rectification ratio. The principal conducting mechanism of the produced n-$CdIn_2Se_4$/Pt thin film Schottky diode is thermionic emission at lower applied biases (≤0.5 V), while the space charge limited conduction mechanism is dominant at higher biases (>0.5 V). The ideality factor values for the n-$CdIn_2Se_4$/Pt thin film Schottky diode are in the range of 1.4819 to 1.8102, depending on the temperature (300 K ≤ $T$ ≤ 342 K). The zero-bias barrier height and effective Richardson's constant of the n-$CdIn_2Se_4$/Pt thin film Schottky diode are ≃0.8652 eV and ≃$1.8771 \times 10^5$ A $m^{-2}$ $K^2$, respectively. The effective density of permitted energy levels is ≃$1.5491 \times 10^{24}$ $m^{-3}$ in the conduction band of the n-$CdIn_2Se_4$ thin films. Additionally, characterization of the voltage–capacitance curve of the n-$CdIn_2Se_4$/Pt thin film Schottky diode revealed its zero bias built-in diffusion potential (≃0.8178 V), donor impurity concentration (≃$5.9132 \times 10^{21}$ $m^{-3}$), and flat-band barrier height (≃0.9525 eV). Based on Anderson's model, several electrical transport parameters were applied to depict the theoretical energy band diagram of the n-$CdIn_2Se_4$/Pt thin film Schottky diode. The functional groups present in the $CdIn_2Se_4$ thin films deposited on a platinum thin film substrate were determined using Fourier transform infrared spectroscopy.

Received 5th August 2025
Accepted 22nd October 2025

DOI: 10.1039/d5ra05715a

rsc.li/rsc-advances



## 1. Introduction

The first systematic study on metal–semiconductor rectifying systems is typically credited to Braun in 1874, who observed that the total resistance of a point contact depends on the specific surface characteristics and the polarity of the applied voltage.[1] Point contact rectifiers have been used practically in various forms since the turn of the nineteenth century. Metal semiconductor contacts have been the subject of much research due to their significance in direct current and microwave applications and their intricate role in other semiconductor devices.[2] In particular, Schottky diode structures have been employed in solar cells as the gate electrode of metal-semiconductor field-effect transistors, photodetectors, and other applications. Above all, the metal contact on strongly doped semiconductors creates an ohmic contact, which is necessary to allow current to flow in and out of all semiconductor devices.[3]

The photoelectrical properties of an Au–$CdIn_2S_4$ surface barrier diode were studied by S. I. Radautsan *et al.*[4] The current transport in p-type $CdIn_2Te_4$ Schottky diodes was studied by S. Kianian *et al.*[5] The fabrication and electrical characterization of an Al/p-$ZnIn_2Se_4$ thin film Schottky diode structure were reported by Dhruv *et al.*[6] Chong Ouyang *et al.* reported the use of a hierarchical $MoO_2$/$ZnIn_2S_4$ Schottky heterojunction to stimulate photocatalytic $H_2$ evolution under visible light.[7]

[a]*Natubhai V. Patel College of Pure and Applied Sciences, The Charutar Vidya Mandal (CVM) University, Vallabh Vidyanagar, 388120, Anand, Gujarat, India. E-mail: dhananjaydhruv@rediffmail.com*

[b]*Department of Nanoscience and Advanced Materials, Saurashtra University, Rajkot 360005, Gujarat, India*

[c]*Laboratory of Magnetic Films Physics, Scientific-Practical Materials Research Centre of National Academy of Sciences of Belarus, 220072 Minsk, Belarus*

[d]*Institute of Automation and Control Processes Far Eastern Branch of the Russian Academy of Sciences, 5 Radio St., Vladivostok 690041, Russia*

[e]*Government Science College, Maharaja Krishnakumarsinhji Bhavnagar University, Gariyadhar, 364505, Bhavnagar, Gujarat, India*

$CdIn_2Se_4$ thin films have been deposited using a range of techniques by different authors, including sol–gel dip coating, hydro evaporation, spray pyrolysis, chemical bath deposition, electrochemical, pulsed electrodeposition, and potentiostatic cathodic electrodeposition.[8–14] Among them, pulsed laser deposition is a great option for depositing ternary semiconducting materials given that its parts have different vapor pressures. Compared to conventional vacuum-based thin film deposition techniques, pulsed laser deposition technology shortens the processing time by facilitating rapid thin film growth, while maintaining homogeneity. The most exciting aspect of pulsed laser deposition technology is its easy manufacture of multilayer devices and heterojunctions, and fine film thickness control. To create $CdIn_2Se_4$ thin films, scientists used pulsed laser deposition given that it has several advantages over traditional thin film deposition techniques, such as maintaining the precise composition of the target material in the formed film. Our extensive review and experimental work on $CdIn_2Se_4$ and/or $CdIn_2Se_4$ thin films[15–17] shows that Hahn *et al.*[18] initially reported work on this ternary semiconducting compound in 1955. After that, no one documented any work on $CdIn_2Se_4$ thin films until 1991. Our rigorous assessment indicates that no one has attempted to construct n-$CdIn_2Se_4$/Pt thin film Schottky diodes using pulsed laser deposition.

The present investigation focuses on optimizing the pulsed laser deposition parameters for the formation of single-phase, polycrystalline, stoichiometric $CdIn_2Se_4$ thin films. The crystal structure and microstructural parameters of $CdIn_2Se_4$ thin films deposited on amorphous quartz glass substrates previously pre-deposited with platinum substrates have been presented. In the case of the $CdIn_2Se_4$ thin film and/or n-$CdIn_2Se_4$/Pt thin film Schottky diode, characterization of their electrical transport was performed to determine their rectification ratio, reverse saturation current, ideality factor, zero-bias barrier height, effective Richardson's constant, effective density of allowed energy states in the conduction band, zero bias built-in diffusion potential, donor impurity concentration, flat-band barrier height, type of conductivity, *etc.* Furthermore, the purity of the $CdIn_2Se_4$ thin films was examined using Fourier transform infrared spectroscopy.

## 2. Experimental

### 2.1 Fabrication of n-$CdIn_2Se_4$/Pt thin film Schottky diode

A schematic illustration of the n-$CdIn_2Se_4$/Pt thin film Schottky diode device under investigation is shown in Fig. 1. A high-purity (≃99.998%) platinum metal (CAS number: 7440-06-4; Merck) thin film with a thickness of about ≃100 nm was deposited at room temperature (≃300 K) on an ultrasonically cleaned amorphous quartz glass (fused silica) (Blue Star, Polar Industries Corporation, India) substrate employing an electron beam evaporation system (model: Auto 500; Hind High Vacuum Co. Pvt. Ltd, India). Using high-purity conductive silver adhesive paste (model: RS pro-RS186-3600; RS Components & Controls Limited, India), a single-phase $CdIn_2Se_4$ (ref. 16) pellet target and amorphous quartz glass substrates pre-deposited with platinum were mounted on the target holder and temperature-controlled substrate holder, respectively, in a stainless-steel pulsed laser deposition chamber (Excel Instruments, India). An ≃100 nm-thick $CdIn_2Se_4$ thin film was then deposited on the pre-deposited platinum thin film substrate at a substrate temperature of ≃550 K using a high-vacuum pulsed laser deposition (model: Compex-Pro Excimer Laser 102F; Coherent, Germany) technique by irradiating the $CdIn_2Se_4$ pellet target with a krypton fluoride pulsed laser. The details of the thin film deposition technique are elaborated elsewhere.[15] Using a suitable mica mask arrangement, the effective cross-sectional area of the n-$CdIn_2Se_4$/Pt thin film Schottky diode device was set to ≃$2.5000 \times 10^{-5}$ $m^2$ (≃8.3 mm length × 3.0 mm breadth).

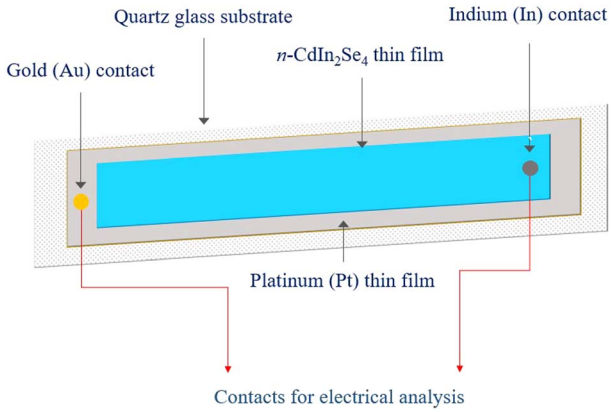


Fig. 1 The structure of the n-$CdIn_2Se_4$/Pt thin film Schottky diode (top view).

Our previous investigation[15] on the deposition and transport characterization of $CdIn_2Se_4$ thin films suggests that their DC electrical resistivity decreases with an increase in the substrate temperature. The DC electrical resistivity reached the lowest value of ≃0.1751 Ω m at a substrate temperature of ≃550 K. Therefore, in the current study, thin films of $CdIn_2Se_4$ were deposited on amorphous quartz glass substrates pre-deposited with platinum at the optimal substrate temperature of ≃550 K.

To produce stoichiometric polycrystalline $CdIn_2Se_4$ thin films, several pulsed laser deposition system parameters have been customized, as indicated in Table 1.

### 2.2 Characterization of n-$CdIn_2Se_4$/Pt thin film Schottky diode

The crystal structure of the $CdIn_2Se_4$ thin films deposited on amorphous quartz glass substrates pre-deposited with platinum

Table 1 Optimized pulsed laser deposition parameters for the synthesis of the $CdIn_2Se_4$ thin films

| Sr. no. | Parameter | Value |
|---|---|---|
| 01 | KrF laser wavelength ($\lambda$) | ≃248 nm |
| 02 | KrF laser energy | ≃249 mJ |
| 03 | Repetition rate (frequency) | ≃4 Hz |
| 04 | Source-to-substrate distance | ≃45 mm |
| 05 | Base pressure (vacuum) | ≃$1.5000 \times 10^{-4}$ Pa |
| 06 | Deposition time (laser ablation time) | ≃4 min |
| 07 | Evaporation rate | ≃10 nm $s^{-1}$ |

using the pulsed laser deposition technique at a substrate temperature of ≃550 K was examined using a grazing incidence X-ray diffractometer (model: SmartLab 9 kW; Rigaku Corporation, Japan) with the typical CuKα radiation at a wavelength of ≃0.1541 nm in the 2$\theta$ diffraction angle range of 20° to 80°. The electrical transport characterization of the n-$CdIn_2Se_4$/Pt thin film Schottky diode was performed using a DC power supply (model: IT6722A; ITech, Taiwan), a digital multimeter (model: DMM 6500 6.5; Keithley, USA), and a semiconductor characterization system (model: SCS-4200; Keithley, USA). At room temperature (≃303 K), a Fourier transform infrared spectrophotometer (model: IRSpirit-X; Shimadzu, Japan) operated in mid-infrared mode in the wavenumber range of 4000–600 $cm^{-1}$ with a resolution of ≃2 $cm^{-1}$ was employed to identify the presence of the functional groups in the $CdIn_2Se_4$ thin films deposited on amorphous quartz glass substrates that had been pre-deposited with platinum at a substrate temperature of ≃550 K.

The electrical transport characterization of the n-$CdIn_2Se_4$/Pt thin film Schottky diode as a function of temperature (300 K ≤ $T$ ≤ 342 K) was conducted inside a glass dome at a low vacuum of ≃1.40 Pa, created using a rotary pump (model: FD12; Hind High Vacuum Co. Pvt. Ltd, India) to prevent contamination from the ambient conditions. All the pulsed laser deposition parameters listed in Table 1 were kept almost constant during the fabrication of the n-$CdIn_2Se_4$/Pt thin film Schottky diode to guarantee the reproducibility of the results, as several pre- and post-deposition parameters can influence the properties of thin films in vacuum technology. The present study analyzed, interpreted, and reported the statistically significant data from the simultaneous fabrication of several n-$CdIn_2Se_4$/Pt thin film Schottky diodes under identical conditions.

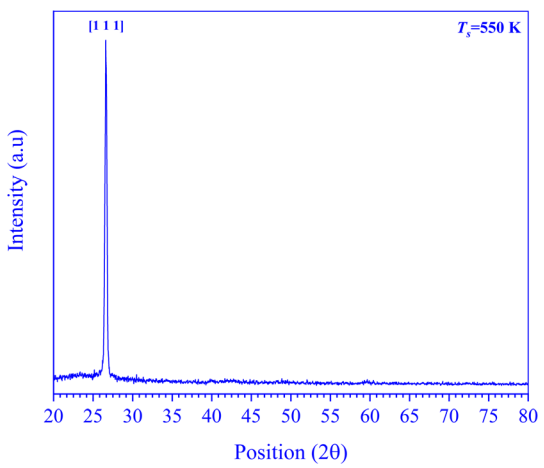


Fig. 2 Typical grazing incidence X-ray diffractogram of the $CdIn_2Se_4$ thin film.

## 3. Results and discussion

### 3.1 Grazing incidence X-ray diffraction (GI-XRD) analysis

The typical grazing incidence X-ray diffractogram in Fig. 2 shows a sharp and intense ⟨1 1 1⟩ characteristic reflection at a diffraction angle of ≃26.60°, indicating that the $CdIn_2Se_4$ thin films deposited on amorphous quartz glass substrates pre-deposited with platinum at a substrate temperature of ≃550 K are polycrystalline; the results are in good agreement with the ICDD 01-089-2388 database for tetragonal (pseudo-cubic) α-phase $CdIn_2Se_4$ with space group $P\bar{4}2m$ ⟨1 1 1⟩ reflections, showing no signs of an elemental or secondary phase.[15,16]

Table 2 displays the microstructural parameters including lattice constant, cell volume, $d$-interplanar spacing, stacking fault, crystallite size, dislocation density, and lattice strain calculated from the grazing incidence X-ray diffractogram pattern for the most noticeable ⟨1 1 1⟩ reflection of the α-$CdIn_2Se_4$ thin films on amorphous quartz glass substrates that had previously been pre-deposited with platinum using the pulsed laser deposition technique at a substrate temperature of ≃550 K.[19]

Using eqn (1) for a tetragonal crystal structure, the lattice constant ($a$) of the α-$CdIn_2Se_4$ thin film (where $a \simeq c$) was determined,[20] as follows:

$$\frac{1}{a^2} = \frac{h^2 + k^2}{a^2} + \frac{l^2}{c^2} \quad (1)$$

In the tetragonal crystal structure, the unit cell volume ($V$) of the α-$CdIn_2Se_4$ thin film can be inferred using the relation $V = a^2c$.[21]

Using Bragg's eqn (2), the $d$-interplanar spacing value of the α-$CdIn_2Se_4$ thin film was determined,[22] as follows:

$$n\lambda = 2d \sin\theta \quad (2)$$

Planar flaws known as stacking faults (SF) disturb the normal arrangement of atomic layers. A higher stacking fault

Table 2 Microstructural parameters of the α-$CdIn_2Se_4$ thin film

| Microstructural parameters | Reported value | Current investigation | Deviation (%) | Reference/Method |
|---|---|---|---|---|
| Lattice constant ($a$) (nm) | 0.5815 | 0.5801 | 0.2408 | ICDD card 01-089-2388 |
| Cell volume ($nm^3$) | 0.1966 | 0.1952 | 0.7121 | ICDD card 01-089-2388 |
| $d_{111}$ (nm) | 0.3357 | 0.3349 | 0.2383 | ICDD card 01-089-2388 |
| Stacking fault ($\times10^{-3}$) | — | 4.62 | — | — |
| Crystallite size (nm) | — | 16.08 | — | Scherrer method |
| Dislocation density ($\times10^{-3}$) (lines per $nm^2$) | — | 3.87 | — | Williamson–Smallman's method |
| Lattice strain ($\times10^{-3}$) | — | 9.37 | — | — |

value introduces localized energy states inside the bandgap, changing the leakage behavior and current flow. Furthermore, a greater stacking fault value may result in a decrease in the rectification efficiency and an increase in the reverse leakage current. The stacking fault value of the α-$CdIn_2Se_4$ thin film can be obtained using eqn (3).[23]

$$SF = \frac{0.2533\beta}{(\tan\theta)^{\frac{1}{2}}} \quad (3)$$

where $\beta$ represents the full breadth/width at half maximum (FWHM) of the diffraction peak in the above-mentioned relation, enabling the determination of the crystallite size ($D$) of the tetragonal α-phase $CdIn_2Se_4$ thin film using the Scherrer eqn (4),[24] as follows:

$$D\beta\cos\theta = K\lambda \quad (4)$$

Dislocation density ($\delta$) is a defect that arises from misaligned atoms in the crystal lattice. It shortens the carrier lifespan by acting as a location for electron and hole recombination. It increases the leakage current, while lowering the breakdown voltage. It could lead to less-than-ideal diode behavior by making the Schottky barrier less uniform. A high dislocation density leads to low device reliability and thermal instability. The dislocation density of the α-$CdIn_2Se_4$ thin film can be obtained by substituting the crystallite size value obtained from the Scherrer method into eqn (5).

$$\delta = \frac{1}{D^2} \quad (5)$$

Strain ($\varepsilon$) is caused by lattice mismatches or differences in thermal expansion between the substrate and the thin film. Strain alters the band structure and carrier mobility. Consequently, uncontrolled strain typically degrades the transport properties. The Stokes–Wilson (S–W) eqn (6) can be employed to determine the lattice strain developed in the α-$CdIn_2Se_4$ thin film due to crystal imperfection and disorder.[25]

$$\beta = 4\varepsilon\tan\theta \quad (6)$$

The low dislocation density, stacking fault, and lattice strain in the fabricated n-$CdIn_2Se_4$/Pt thin film Schottky diode could be the factors responsible for the enhanced performance of the thin film Schottky diode device in this work.

### 3.2 Hall effect analysis

The $CdIn_2Se_4$ thin film produced at a substrate temperature of $\simeq$550 K consistently exhibited n-type conductivity, according to hot probe tests. When recorded at a magnetic field of $\simeq$0.2001 T, Hall measurements yielded a negative Hall coefficient value of $\simeq -0.4488 \times 10^{-3}$ $m^3$ $C^{-1}$, which is consistent with the findings of hot probe testing and suggests that the majority of charge carriers are electrons.[26] According to the Hall measurements, the donor impurity concentration in the n-type $CdIn_2Se_4$ thin films is $\simeq 7.1300 \times 10^{21}$ $m^{-3}$.[15]

### 3.3 Voltage–current characteristics

Fig. 3 shows the sweep forward and reverse biased electrical transport characterization of the n-$CdIn_2Se_4$/Pt thin film Schottky diode at various ambient temperatures (300 K $\leq T \leq$ 342 K). The rectifying electrical transport characteristic evident in Fig. 3 confirms the formation of a typical diode-type junction between n-$CdIn_2Se_4$/Pt, signifying the formation and presence of a depletion width between the n-type $CdIn_2Se_4$ semiconducting material and tungsten metal, which in turn restricts the flow of forward- and reverse-charge carriers at the intersection region.[27]

According to Table 3, the rectification ratio of the n-$CdIn_2Se_4$/Pt thin film Schottky diode increases when the ambient temperature decreases (300 K $\leq T \leq$ 342 K) and the bias is constant; when the ambient temperature remains constant, the rectification ratio increases as the bias increases. Constrained deficiencies in the intersection zone and the increase in the leakage current with an increase in ambient temperature may be two ways to describe this effect.[28,29]

The effective evaluation of the current conduction processes in all manufactured semiconducting thin film electronic devices requires a detailed examination of their electrical transport characteristics. The electrical transport characterization reveals two current conduction regions, *i.e.*, a rectifying region at a higher applied bias and a practically ohmic region at a lower applied bias. Ohmic behaviour results from the inserted charge carrier density being less than the thermally generated carrier density at a lower applied bias. The trap-controlled space charge limiting current/conduction mechanism predominates in this region given that the slope is greater than two with a higher applied bias.[28]

To learn more about the current conduction mechanism in the n-$CdIn_2Se_4$/Pt thin film Schottky diode at a lower applied bias (≤0.5 V), as well as to determine the reverse saturation current and ideality factor, the model put forth by Sze and

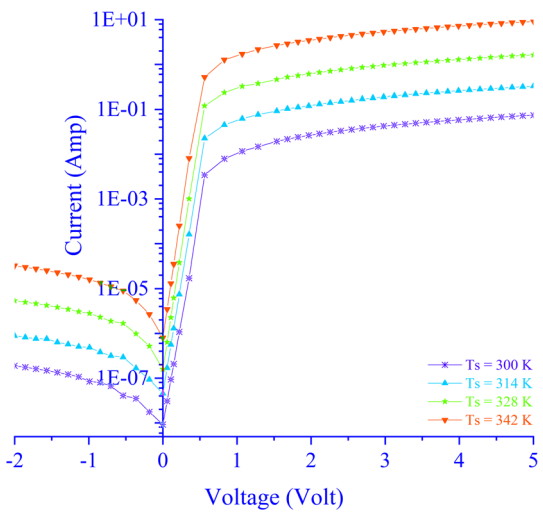


Fig. 3 Electrical transport characterization of the n-$CdIn_2Se_4$/Pt thin film Schottky diode.

Table 3 Rectification ratio of the n-$CdIn_2Se_4$/Pt thin film Schottky diode

| Temperature (K) | Rectification ratio ($\times 10^5$) | | | | | | | |
|---|---|---|---|---|---|---|---|---|
| | Applied bias (V) | | Applied bias (V) | | Applied bias (V) | | Applied bias (V) | |
| | −2.0011 | +1.9690 | −1.5682 | +1.5362 | −0.9904 | +1.0705 | −0.5371 | +0.5638 |
| 300 | 1.4178 | | 1.3328 | | 1.2762 | | 0.7974 | |
| 314 | 1.3770 | | 1.2525 | | 1.1936 | | 0.7381 | |
| 328 | 1.1584 | | 1.1152 | | 1.0689 | | 0.6901 | |
| 342 | 1.0798 | | 1.0672 | | 0.9914 | | 0.5489 | |

Crowell[3] was used and fitted in the current investigation. Eqn (7) illustrates how the applied bias alters the current.

$$\frac{I}{I_s} = \exp\left(\frac{qV}{nkT}\right) \quad (7)$$

In eqn (7), $\frac{KT}{q}$ is the thermal voltage ($\simeq 0.0259$ V) at $\simeq 300$ K.

Fig. 4 shows the variation in natural logarithmic current for a constructed n-$CdIn_2Se_4$/Pt thin film Schottky diode at different ambient temperatures with an applied bias ($\leq$0.5 V). With an increase in the applied bias ($\leq$0.5 V), the forward current of the constructed n-$CdIn_2Se_4$/Pt thin film Schottky diode increases exponentially, as demonstrated by the linear-straight-line curve in Fig. 4. Also, the linear-straight-line plot indicates that the main characteristic of the produced n-$CdIn_2Se_4$/Pt thin film Schottky diode is thermionic emission at a lower applied voltage ($\leq$0.5 V).[6] The ideality factors of the n-$CdIn_2Se_4$/Pt thin film Schottky diode at different ambient temperatures were determined using the slope values, and the reverse saturation currents were derived from the linear-straight-line intercept values shown in Fig. 4.

The reverse saturation current and ideality factor at various ambient temperatures are displayed in Table 4.

In a thin film Schottky diode made of metal and semiconductor, its reverse saturation current mainly depends on the ambient temperature $\left[I_s = T^3 \exp\left(-\frac{E_g}{kT}\right)\right]$, whereas it is not affected by the reverse voltage.[3]

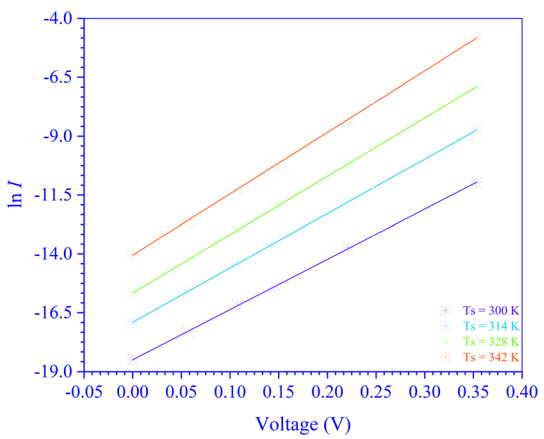


Fig. 4 The variation in ln *I* with applied bias for the n-$CdIn_2Se_4$/Pt thin film Schottky diode.

Temperature has a much more noticeable effect because thin films have greater grain boundaries and defect concentrations, which encourage the generation of carriers.[30] Consequently, the reverse saturation current decreases as the ambient temperature decreases because fewer minority charge carriers are in the depletion width. The ideality factor of a diode shows how well it follows the ideal diode formula. The ideality factor value typically ranges from one, which indicates ideal diffusion, to two, which indicates dominant recombination. Because recombination predominates in the depletion region, the ideality factor values get closer to two at lower temperatures. As the temperature increases, the ideality factor gets closer to one because recombination decreases and the diffusion current increases. The ideality factor value is observed at low and/or high ambient concentrations; however, it substantially changes as the doping concentration increases and/or the ambient temperature decreases. The ideality factor shifts in thin films at high temperatures due to the increased carrier mobility and decreased trap-assisted recombination.[31]

Eqn (8) was utilized to analyze the current conduction mechanism in the n-$CdIn_2Se_4$/Pt thin film Schottky diode at a lower applied bias ($\leq$0.5 V), as well as to determine the zero-bias barrier height and effective Richardson's constant values.[32]

$$\frac{AA^*T^2}{I_s} = \exp\left(\frac{q\varphi_b}{kT}\right) \quad (8)$$

In eqn (8), $A$ is the effective cross-sectional area of the n-$CdIn_2Se_4$/Pt thin film Schottky diode. The effective Richardson's constant $\left(A^* = \frac{4\pi q m_n k^2}{h^3}\right)$ is an effective mass-dependent parameter.

The linear-straight-line character of Fig. 5 suggests a thermionic emission conduction mechanism in the n-$CdIn_2Se_4$/Pt thin film Schottky diode at lower applied voltages (<0.5 V).

Table 4 Temperature-dependent electrical parameters of the n-$CdIn_2Se_4$/Pt thin film Schottky diode

| Temperature (K) | Intercept | Reverse saturation current ($\times 10^{-9}$) (A) | Slope | Ideality factor |
|---|---|---|---|---|
| 300 | −18.50560 | 9.1859 | 21.3617 | 1.8102 |
| 314 | −16.90890 | 45.3480 | 23.1085 | 1.6734 |
| 328 | −15.66250 | 157.7100 | 24.7977 | 1.5594 |
| 342 | −14.05760 | 784.9900 | 26.0940 | 1.4819 |

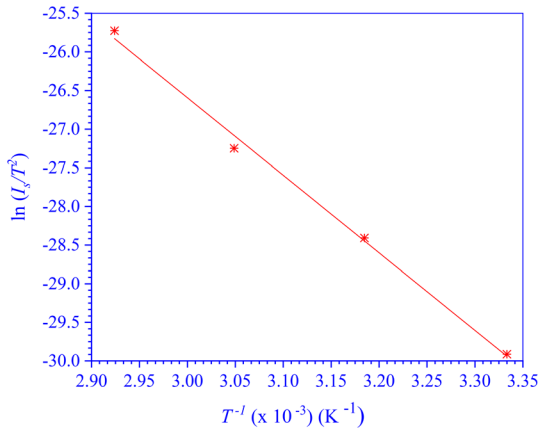


Fig. 5 $\ln\left(\frac{I_S}{T^2}\right)$ *versus* $\frac{1000}{T}$ plot of the n-$CdIn_2Se_4$/Pt thin film Schottky diode.

The zero-bias barrier height of the n-$CdIn_2Se_4$/Pt thin film Schottky diode is determined using the slope in Fig. 5 and found to be $\simeq$0.8652 eV. The intercept extracted from Fig. 5 gives the effective Richardson's constant $\simeq 1.8771 \times 10^5$ A $m^{-2}$ $K^2$ for the $CdIn_2Se_4$ thin films grown at a substrate temperature of $\simeq$550 K, which is equivalent to 0.1562 $m_0$. The room temperature effective mass values of n-type $CdIn_2Se_4$ reported by various other authors are 0.15 $m_0$,[33,34] 0.1600 $m_0$,[34] and 0.1780 $m_0$.[35]

By inserting the effective mass of n-type $CdIn_2Se_4$ and other commonly reported values, it is possible to determine that the effective density of allowed energy states in the conduction band $\left(= 2\left[\frac{2\pi m_n kT}{h^2}\right]^{\frac{3}{2}}\right)$ is similarly an effective mass-dependent characteristic, which is $\simeq 1.5491 \times 10^{24}$ $m^{-3}$. The deduced effective density of allowed energy states in the conduction band is consistent with the values published by Bhalerao *et al.*[10]

To verify the current conduction mechanism at a higher bias (>0.5 V), a natural logarithmic current was recorded against applied bias (>0.5 V) at varying ambient temperatures, as shown in Fig. 6(a). At a greater bias (>0.5 V), the rectifying nature of the plot in Fig. 6(a) suggests a variable current conduction mechanism for the n-$CdIn_2Se_4$/Pt thin film Schottky diodes.

Fig. 6(b) illustrates the change in current against the square of the applied bias at a greater applied bias (>0.5 V). Fig. 6(b) shows straight line character, supporting the space charge restricted current/conduction mechanism of the n-$CdIn_2Se_4$/Pt thin film Schottky diode.[28] The space charge restricted current/conduction mechanism is dominated by charge carriers injected from the contacts; the current is solely dependent on mobility and not on the density of the charge carriers, and the voltage–current characteristics follow a second-degree polynomial relation.

### 3.4 Voltage–capacitance characteristics

The change in capacitance with applied bias was recorded at a frequency of 500 kHz at room temperature to extract several

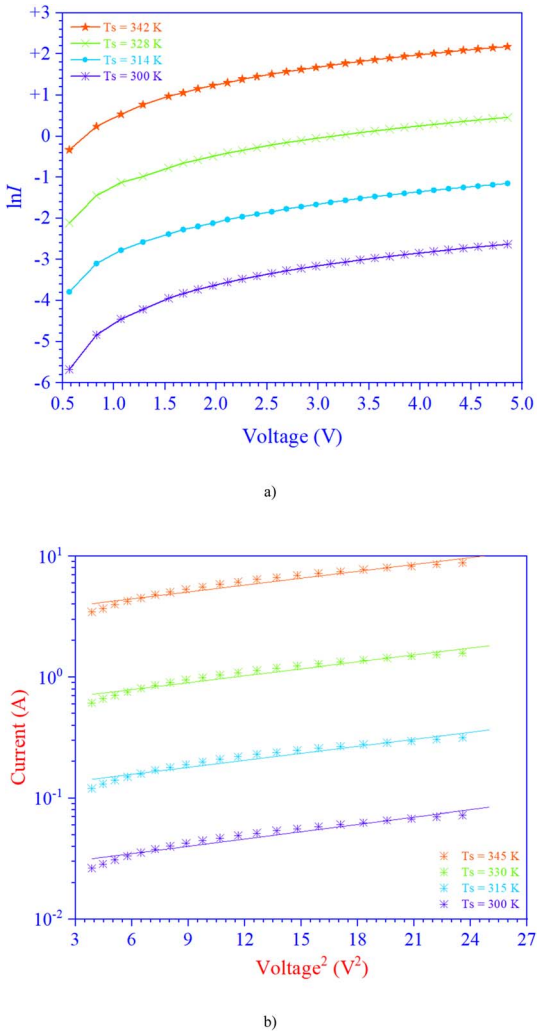


Fig. 6 The variation in current with applied bias (>0.5 V) for the n-$CdIn_2Se_4$/Pt thin film Schottky diode.

important parameters, including the zero-bias built-in diffusion potential, donor impurity concentration, flat-band barrier height, and type of conductivity of the n-$CdIn_2Se_4$ thin film and/or n-$CdIn_2Se_4$/Pt thin film Schottky diode. Eqn (9) establishes an empirical relationship between applied bias and junction capacitance.[32]

$$\frac{1}{2C^2} = \frac{\left(V - V_0 + \frac{kT}{q}\right)}{q\varepsilon_0\varepsilon_r N_D A^2} \quad (9)$$

In eqn (9), $V_0$ is the zero bias built-in diffusion potential ($\simeq$0.8178 V), which may be possibly due to the non-homogeneous surface states in the system, $\varepsilon_r$ is the relative dielectric constant of n-$CdIn_2Se_4$ ($\simeq$6.2000 (ref. 36)), and $N_D$ is the donor impurity concentration.

The donor impurity concentration of the n-$CdIn_2Se_4$ thin films is $\simeq 5.9132 \times 10^{21}$ $m^{-3}$, as inferred from the slope $\left(\simeq 6.1529 \times 10^{16}\frac{F^{-2}}{V} = \frac{2}{q\varepsilon_0\varepsilon_r N_D A^2}\right)$ of the inverse of the square of capacitance *vs.* applied bias plot in Fig. 7. The donor impurity

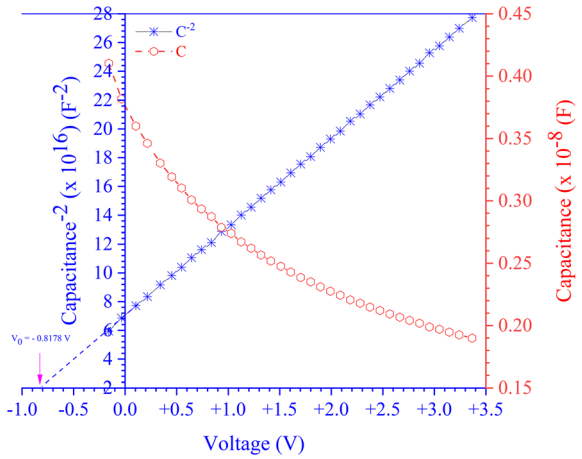


Fig. 7 Variation in capacitance as a function of the bipolar voltage for the n-$CdIn_2Se_4$/Pt thin film Schottky diode.

concentration ($\simeq 7.1300 \times 10^{21}$ $m^{-3}$) derived from the voltage–capacitance measurements and Hall effect tests is in close agreement with the donor impurity concentration in n-$CdIn_2Se_4$ thin films reported by Bhalerao *et al.*[10]

One can use eqn (10) to determine the flat-band barrier height of the n-$CdIn_2Se_4$/Pt thin film Schottky diode,[28] as follows:

$$\left(\varphi_b - V_0 - V_n = \frac{kT}{q} - \Delta\phi_B\right) \quad (10)$$

In eqn (10), $V_n$ ($\simeq E_C - E_{Fn}$) is the potential difference between the conduction band (CB) ($E_C$) and Fermi level ($E_{Fn}$) in n-type $CdIn_2Se_4$. Using eqn (11),[37] the value of $V_n$ is calculated to be $\simeq 0.1440$ V, which is extremely close to the $V_n$ ($\simeq 0.1430$ V) value reported by Bhalerao *et al.*[10]

$$\frac{N_C}{N_D} = \exp\left(\frac{qV_n}{kT}\right) \quad (11)$$

It is necessary to consider an appropriate interface electric field when a metal and a semiconductor come into contact, and to substitute the dielectric constant of the semiconductor ($\simeq 6.2000$ for n-$CdIn_2Se_4$)[36] for the free space dielectric constant. Eqn (12) expresses the reduction in the Schottky barrier height.[6]

When a metal is in contact with a semiconductor, the appropriate interface electric field has to be considered, and the free space dielectric constant has to be replaced by the dielectric constant of the semiconductor ($\simeq 6.2000$ (ref. 36) for n-$CdIn_2Se_4$). The Schottky barrier image force barrier lowering can be expressed by employing eqn (12),[3]

$$\Delta\phi_B = \left(\frac{qE_m}{4\pi\varepsilon_0\varepsilon_s}\right)^{\frac{1}{2}} \quad (12)$$

Eqn (13) can be used to deduce the maximum electric field at the n-$CdIn_2Se_4$/Pt thin film Schottky diode junction. The derived value is $\simeq 5.3129 \times 10^6$ V $m^{-1}$.[3]

$$E_m = \left(\frac{2qN_D V_0}{\varepsilon_0\varepsilon_s}\right)^{\frac{1}{2}} \quad (13)$$

In the case of the n-$CdIn_2Se_4$/Pt thin film Schottky diode, its Schottky barrier image force barrier lowering value deduced from eqn (12) is $\simeq 3.5128 \times 10^{-2}$ V.

By substituting $V_n \simeq 0.1440$ V, $V_0 \simeq 0.8178$ V, and $\Delta\phi_B$ into eqn (10), the flat-band barrier height for the n-$CdIn_2Se_4$/Pt thin film Schottky diode is found to be $\simeq 0.9525$ eV.

In contrast to the flat-band barrier height result from the voltage–capacitance experiment ($\simeq 0.9525$ eV), the zero-bias barrier height from the voltage–current measurement ($\simeq 0.8652$ eV) is tiny. This discrepancy in the barrier height results between the two approaches may be due to the edge leakage current, deep impurity levels, or interface contamination.[38]

### 3.5 Energy band diagram construction for n-$CdIn_2Se_4$/Pt thin film Schottky diode

The conductance of current and its capacitance behaviour are controlled by the barrier at the metal-semiconductor interface when metal comes into contact with a semiconductor.[3] The fundamental energy band diagram that forms the barrier height and certain effects that can alter its value are examined in this section.

Firstly, the ideal scenario is considered, which is free of anomalies such as interface states. The electrical energy relation between the n-type $CdIn_2Se_4$ semiconductor and high work function platinum metal, which are in different systems and not in contact, are depicted in Fig. 8(a).

Charge will move from the n-type $CdIn_2Se_4$ semiconducting material to the platinum metal when communication between them is permitted, as seen in Fig. 8(b), and thermal equilibrium is reached as a single system. Both the n-type $CdIn_2Se_4$ and platinum sides will have matching Fermi values. The contact potential, or difference between the two work functions, lowers the Fermi level in the n-type $CdIn_2Se_4$ semiconductor by a value equivalent to the Fermi level in the platinum metal. The work functions of the n-type $CdIn_2Se_4$ semiconducting material and platinum metal are $\simeq 4.1858$ eV and $\simeq 5.1200$ eV, respectively.[33] A contact potential of $\simeq 0.9342$ eV is found. The barrier height in the n-$CdIn_2Se_4$/Pt thin film Schottky diode is determined to be $\simeq 1.0782$ eV, which is determined by the difference between the platinum metal work function and the electron affinity of the n-type $CdIn_2Se_4$ semiconducting material ($\simeq 4.0418$ eV).

### 3.6 Fourier transform infrared (FTIR) spectroscopy analysis

In the present investigation, only 5N (99.999%) pure cadmium, indium, and selenium were used to synthesize $CdIn_2Se_4$.[16] After that, $CdIn_2Se_4$ was deposited on amorphous quartz glass substrates that had already been coated with platinum using pulsed laser deposition, a non-chemical thin film deposition method.

Fig. 9 displays the Fourier transform infrared spectrum of the n-type $CdIn_2Se_4$ thin films deposited at a substrate temperature of $\simeq 550$ K on amorphous quartz glass substrates

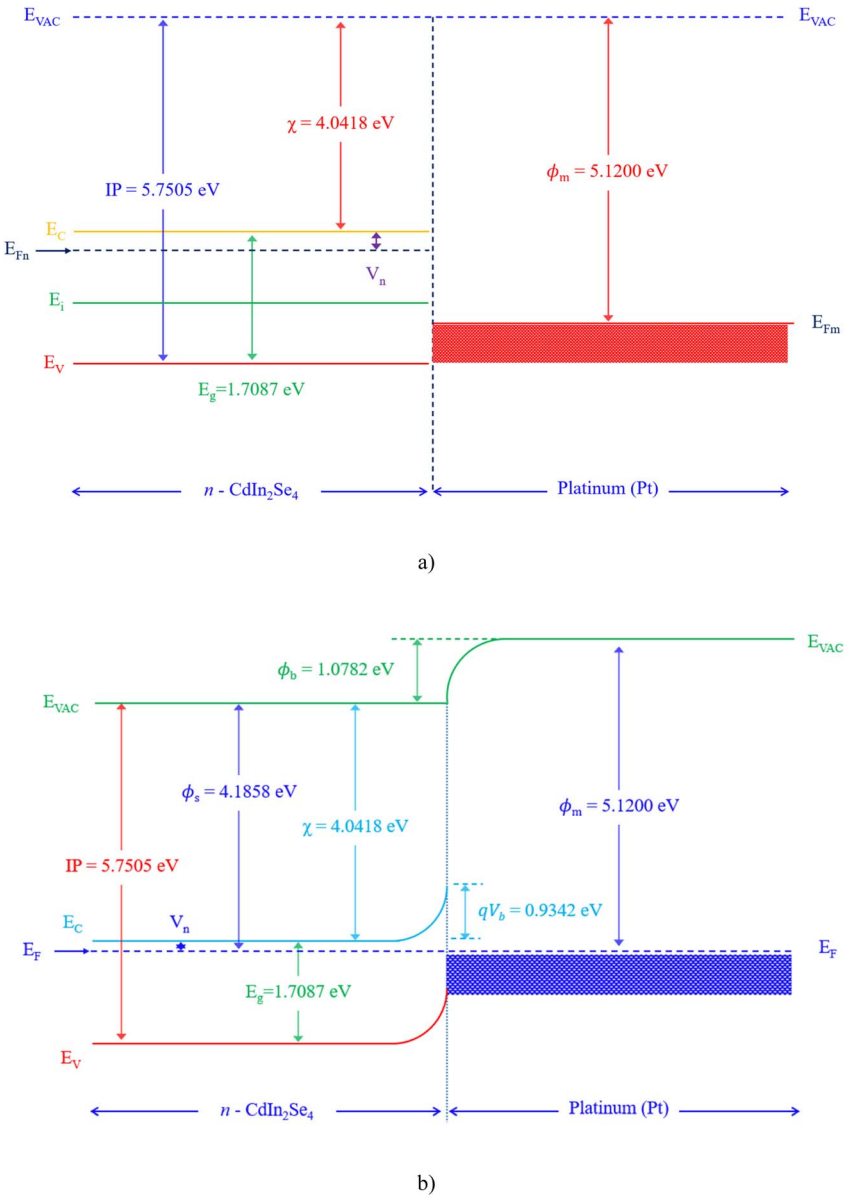


Fig. 8 Energy band diagram of the n-$CdIn_2Se_4$/Pt thin film Schottky diode: (a) isolated and (b) constructed.

that had been pre-deposited with platinum. The spectrum was recorded in the wavenumber ($\bar{\nu}$) range of 4000 to 400 $cm^{-1}$ at room temperature ($\simeq$300 K). Cartesian coordinates have been used to represent the position of the peaks; for instance, 711.8757 indicates the wavenumber ($\bar{\nu}$) and 0.0148 denotes the absorbance.

The peak depicted at a wavenumber of $\simeq$711.8757 $cm^{-1}$ can be attributed to the alkene class bending C=C functional group. The fluoro compound class stretching C–F functional group is responsible for the peaks observed at wavenumbers of $\simeq$1036.2383 $cm^{-1}$, $\simeq$1266.5933 $cm^{-1}$, and $\simeq$1387.8705 $cm^{-1}$. The nitro compound class stretching N–O functional group is responsible for the peak depicted at a wavenumber of $\simeq$1516.3238 $cm^{-1}$. The aromatic compound class bending C–H functional group corresponds to the peaks detected at wavenumbers of $\simeq$1746.6788 $cm^{-1}$, $\simeq$1905.9896 $cm^{-1}$, and $\simeq$1990.6684 $cm^{-1}$. The isothiocyanate class stretching N=C=S functional group is responsible for the peaks detected at wavenumbers of $\simeq$2076.0648 $cm^{-1}$ and $\simeq$2108.3575 $cm^{-1}$. The carboxylic class stretching O–H functional group can cause the peak detected at a wavenumber of $\simeq$2524.5751 $cm^{-1}$. The stretching O–H functional group in the phenol and/or alcohol class explains the peaks observed at wavenumbers of $\simeq$3532.8264 $cm^{-1}$, $\simeq$3717.2539 $cm^{-1}$, and $\simeq$3784.7099 $cm^{-1}$. The absorption peaks resulting from bending C=C, stretching C–F, stretching N–O, bending C–H, stretching N=C=S, and stretching O–H functional groups usually show strong and/or sharp absorption edges. It can be concluded that the $CdIn_2Se_4$ thin films deposited by pulsed laser deposition on amorphous quartz glass substrates pre-deposited with platinum at

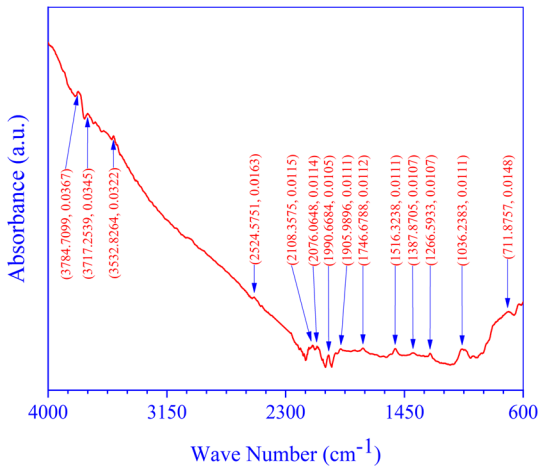


Fig. 9 Fourier transform infrared spectrum of the n-$CdIn_2Se_4$ thin film.

a substrate temperature of ≃550 K are pure and free of any functional groups because the absorption edges visible in the Fourier transform infrared spectrum of $CdIn_2Se_4$ are very weak.[8,39]

## 4. Conclusions

Using a high-vacuum pulsed laser deposition approach, an ≃100 nm-thick $CdIn_2Se_4$ thin film was deposited on amorphous quartz glass substrates that had previously been pre-deposited with platinum at a substrate temperature of ≃550 K. A sharp and intense ⟨1 1 1⟩ characteristic reflection is seen in the typical grazing incidence X-ray diffractogram at a diffraction angle of ≃26.60°, suggesting the polycrystalline nature of the $CdIn_2Se_4$ thin films. The unit cell (≃0.5801 nm), cell volume (≃0.1952 nm$^3$), $d_{111}$ (≃0.3349 nm), stacking fault (≃4.62 × $10^{-3}$), crystallite size (≃16.08 nm), dislocation density (≃3.87 × $10^{-3}$ lines per nm$^2$), and lattice strain (≃9.37 × $10^{-3}$) were all calculated for the $CdIn_2Se_4$ thin films from the most prominent ⟨1 1 1⟩ reflection in the GI-XRD. The n-type conductivity of the $CdIn_2Se_4$ thin films was verified by Hall measurement analysis. A typical Schottky diode-type junction between $CdIn_2Se_4$ and platinum with a fair rectification ratio is confirmed by the voltage–current characterization of the vacuum-fabricated n-$CdIn_2Se_4$/Pt thin film Schottky diode. At a lower applied bias (≤0.5 V), the primary conducting mechanism in the manufactured n-$CdIn_2Se_4$/Pt thin film Schottky diode is thermionic emission, whereas at a higher bias (>0.5 V), the space charge limited conduction mechanism is dominant. The ideality factor values for the n-$CdIn_2Se_4$/Pt thin film Schottky diode vary from 1.4819 to 1.8102, depending on temperature (300 K ≤ $T$ ≤ 342 K). The zero-bias barrier height and effective Richardson's constant were determined to be ≃0.8652 eV and ≃1.8771 × $10^5$ A m$^{-2}$ K$^2$ (≃0.1562 $m_0$), respectively, for the n-$CdIn_2Se_4$/Pt thin film Schottky diode. In the conduction band, the effective density of allowed energy states for the n-$CdIn_2Se_4$ thin films is ≃1.5491 × $10^{24}$ m$^{-3}$. The voltage–capacitance characterization of the n-$CdIn_2Se_4$/Pt thin film Schottky diode yielded its flat-band barrier height (≃0.9525 eV), donor impurity concentration (≃5.9132 × $10^{21}$ m$^{-3}$), and zero bias built-in diffusion potential (≃−0.8178 V). Based on Anderson's model, different electrical transport parameters were employed to plot the theoretical energy band diagram for the n-$CdIn_2Se_4$/Pt thin film Schottky diode. The functional groups (if any) present in the $CdIn_2Se_4$ thin films deposited on a platinum thin film substrate were extracted using Fourier transform infrared spectroscopy.

## Author contributions

All writers contributed to the conceptualization and design of the study. Material preparation, data gathering, and analysis were performed by S. D. Dhruv, Tanvi Dudharejiya, Sergei A. Sharko, Aleksandra I. Serokurova, Nikolai N. Novitskii, D. L. Goroshko, Parth Rayani, Jagruti Jangale, J. H. Markna, Bharat Kataria, and D. K. Dhruv. D. K. Dhruv wrote the first draft of the manuscript, and all authors commented on the previous versions. All authors read and approved the final manuscript. S. D. Dhruv: methodology. Tanvi Dudharejiya: data curation. Sergei A. Sharko: investigation. Aleksandra I. Serokurova: formal analysis. Nikolai N. Novitskii: visualization. D. L. Goroshko: writing – review & editing. Parth Rayani: resources. Jagruti Jangale: validation. J. H. Markna: software. Bharat Kataria: conceptualization. D. K. Dhruv: writing – original draft, supervision, project administration.

## Conflicts of interest

The authors have no related financial or non-financial interests to disclose. The submitted work is the authors' original research and has not been communicated elsewhere for publication. On behalf of all the co-authors, I declare no conflict of interest.

## Data availability

The authors declare that the data supporting the findings of this study are available/included in the main text of the paper.

## Acknowledgements

This work was supported by the Department of Science & Technology (DST), Government of India, New Delhi (File number: DST/INT/BLR/P-36/2023) and the Belarusian Republican Foundation for Fundamental Research (File number: F23INDG-005) under the India-Belarus Programme of Co-operation in Science & Technology (Joint Research Project). The authors thank the Sophisticated Instrumentation Centre for Applied Research and Testing (SICART), Vallabh Vidyanagar-388120, Anand, Gujarat, India, for providing the FTIR spectrophotometer facility at a nominal rate.

## References

1 F. Braun, in *Semiconductor Devices: Pioneering Papers*, World Scientific, 1991, pp. 377–380.

2 E. H. Rhoderick and R. H. Williams, *Metal-semiconductor Contacts*, Clarendon Press ; Oxford University Press, Oxford [England]: New York, 2nd edn, 1988.
3 S. M. Sze and K. K. Ng, *Physics of Semiconductor Devices*, Wiley, 1st edn, 2006.
4 S. I. Radautsan, I. P. Molodyan, S. V. Bulyarskii, N. N. Syrbu and V. E. Tezlevan, *Phys. Status Solidi A*, 1974, **21**, 617–622.
5 S. Kianian, S. A. Eshraghi, O. M. Stafsudd and A. L. Gentile, *J. Appl. Phys.*, 1987, **62**, 1500–1502.
6 D. K. Dhruv and B. H. Patel, *Mater. Sci. Semicond. Process.*, 2016, **54**, 29–35.
7 C. Ouyang, W. Huang, H. Tang, W. Liu, X. Gu, Z. Hong and M. Zhi, *ACS Appl. Energy Mater.*, 2022, **5**, 12739–12751.
8 A.-A. Ruanthon, T. Sarakonsri and C. Thanachayanont, *Funct. Mater. Lett.*, 2009, **02**, 199–203.
9 D. Sudha, S. Dhanapandian, C. Manoharan and A. Arunachalam, *Results Phys.*, 2016, **6**, 599–605.
10 A. B. Bhalerao, B. G. Wagh, R. N. Bulakhe, P. R. Deshmukh, J.-J. Shim and C. D. Lokhande, *J. Photochem. Photobiol., A*, 2017, **336**, 69–76.
11 M. R. Asabe and V. P. Ubale, *International Journal of Engineering Science Invention*, 2013, **2**, 41–44.
12 N. M. Khusayfan, *Aust. J. Basic Appl. Sci.*, 2012, **6**, 329–336.
13 V. M. Nikale, N. S. Gaikwad, K. Y. Rajpure and C. H. Bhosale, *Mater. Chem. Phys.*, 2003, **78**, 363–366.
14 T. Mahalingam, S. Thanikaikarasan, R. Chandramohan, K. Chung, J. P. Chu, S. Velumani and J.-K. Rhee, *J. Mater. Sci. Eng. B*, 2010, **174**, 236–241.
15 S. D. Dhruv, T. Dudharejiya, S. A. Sharko, A. I. Serokurova, N. N. Novitskii, D. L. Goroshko, R. Banerjee, J. Jangale, P. Rayani, V. Solanki, M. P. Deshpande, J. H. Markna, B. Kataria and D. K. Dhruv, *Appl. Phys. A*, 2025, **131**, 663.
16 S. D. Dhruv, S. A. Sharko, A. I. Serokurova, N. N. Novitskii, D. L. Goroshko, P. Rayani, J. Jangale, N. Agrawal, V. Solanki, J. H. Markna, B. Kataria and D. K. Dhruv, *RSC Adv.*, 2025, **15**, 14859–14875.
17 S. D. Dhruv, T. Dudharejiya, S. A. Sharko, A. I. Serokurova, N. N. Novitskii, D. L. Goroshko, P. Rayani, J. Jangale, V. Solanki, P. B. Patel, U. B. Trivedi, J. H. Markna, B. Kataria and D. K. Dhruv, *RSC Adv.*, 2025, **15**, 26353–26361.
18 H. Hahn, G. Frank, W. Klingler, A. D. Störger and G. Störger, *Z. Anorg. Allg. Chem.*, 1955, **279**, 241–270.
19 D. K. Dhruv, B. H. Patel, S. D. Dhruv, P. B. Patel, U. B. Trivedi and N. Agrawal, *Mater. Today: Proc.*, 2023, S2214785323002638.
20 S. D. Dhruv, J. Kolte, P. Solanki, M. P. Deshpande, V. Solanki, J. Tailor, N. Agrawal, V. A. Patel, J. H. Markna, B. Kataria and D. K. Dhruv, *RSC Adv.*, 2024, **14**, 15455–15467.
21 M. A. M. Seyam, G. F. Salem and S. N. A. Aziz, *Egypt. J. Solid.*, 2011, **34**, 88–98.
22 B. D. Cullity and S. R. Stock, *Elements of X-Ray Diffraction*, Prentice Hall, Upper Saddle River, NJ, 3rd edn, 2001.
23 R. Suresh, V. Ponnuswamy and R. Mariappan, *Appl. Surf. Sci.*, 2013, **273**, 457–464.
24 A. El-Habib, M. Addou, A. Aouni, M. Diani, J. Zimou and H. Bakkali, *Materialia*, 2021, **18**, 101143.
25 B. Parveen, Mahmood-ul-Hassan, Z. Khalid, S. Riaz and S. Naseem, *J. Appl. Res. Technol.*, 2017, **15**, 132–139.
26 V. M. Nikale, S. S. Shinde, A. R. Babar, C. H. Bhosale and K. Y. Rajpure, *Sol. Energy*, 2011, **85**, 1336–1342.
27 A. A. Attia, H. A. M. Ali, G. F. Salem, M. I. Ismail and F. F. Al-Harbi, *Opt. Mater.*, 2017, **66**, 480–486.
28 D. K. Dhruv, B. H. Patel, N. Agrawal, R. Banerjee, S. D. Dhruv, P. B. Patel and V. Patel, *J. Mater. Sci.: Mater. Electron.*, 2022, **33**, 24003–24015.
29 D. K. Dhruv, B. H. Patel and D. Lakshminarayana, *Mater. Res. Innovations*, 2016, **20**, 285–292.
30 P. Singh and N. M. Ravindra, *Sol. Energy Mater. Sol. Cells*, 2012, **101**, 36–45.
31 A. D. Dhass, Y. Prakash and K. C. Ramya, *Mater. Today: Proc.*, 2020, **33**, 732–735.
32 A. Seçkin and H. Koralay, *ACS Omega*, 2025, **10**, 6520–6533.
33 O. Madelung, *Semiconductors: Data Handbook*, Springer Berlin Heidelberg, Berlin, Heidelberg, 2004.
34 L. S. Koval, E. K. Arushanov and S. I. Radautsan, *Phys. Status Solidi A*, 1972, **9**, K73–K75.
35 A. Priyambada, A. Mohanty and P. Parida, *Mater. Today Commun.*, 2023, **37**, 107338.
36 H. Neumann, W. Kissinger and F. Lévy, *Cryst. Res. Technol.*, 1990, **25**, 1189–1193.
37 R. D. Jones, *Hybrid Circuit Design and Manufacture*, CRC Press, 1st edn, 2020.
38 Ç. Bilkan and Ş. Altındal, *J. Alloys Compd.*, 2017, **708**, 464–469.
39 Z. H. Mahmoud, Y. Ajaj, A. M. Hussein, H. N. K. Al-Salman, M. A. Mustafa, E. H. Kadhum, S. Abdullaev, S. A. Khuder, G. K. Ghadir, S. M. Hameed, K. Muzammil, S. Islam and E. Kianfar, *Int. J. Biol. Macromol.*, 2024, **267**, 131465.